Dyes and Pigments 86 (2010) 15–24

Contents lists available at ScienceDirect

Dyes and Pigments

journal homepage: www.elsevier.com/locate/dyepig

Protolytic fluorescein species evaluated using chemometry and DFT studies

Vagner Roberto Batistela [a], Jaime da Costa Cedran [b], Hueder Paulo Moisés de Oliveira [c], Ieda Spacino Scarminio [d], Leonardo Tsuyoshi Ueno [e], Antonio Eduardo da Hora Machado [f], Noboru Hioka [b,*]

[a] Centro de Tecnologia, Universidade Estadual de Maringá, Umuarama, Paraná, Brazil
[b] Departamento de Química, Universidade Estadual de Maringá, Av, Colombo, 5.790; CEP 87.020-900 Maringá, Paraná, Brazil
[c] Universidade Camilo Castelo Branco, S. José dos Campos, São Paulo, Brazil
[d] Departamento de Química, Laboratório de Quimiometria em Ciências Naturais, Universidade Estadual de Londrina, Londrina, Paraná, Brazil
[e] Faculdade de Ciências Integradas do Pontal, Laboratório de Química Teórica Computacional, Universidade Federal de Uberlândia, Ituiutaba, Minas Gerais, Brazil
[f] Instituto de Química, Laboratório de Fotoquímica, Universidade Federal de Uberlândia, Uberlândia, Minas Gerais, Brazil

ARTICLE INFO

Article history:
Received 28 September 2009
Received in revised form
16 November 2009
Accepted 19 November 2009
Available online 24 November 2009

Keywords:
Fluorescein
Xanthene
pKa
Principal component analysis
Density functional theory
Chemometry

ABSTRACT

Fluorescein (C.I. Solvent Yellow 94) contains three acid-base groups that lead to a protolytic equilibrium involving four species namely, dianionic, monoanionic, neutral and cationic. Since these species display superimposed bands in their electronic absorption spectra and close pKa values, the determination of pKa using traditional methods is complex. By applying chemometric tools, principal component and Q factor analysis followed by varimax and Imbrie oblique rotations, pKa values in water, $pKa_1 = 2.5$, $pKa_2 = 3.8$ and $pKa_3 = 6.1$, were obtained. Geometric parameters secured using Density Functional Theory combined with a polarized continuum model that simulates the surrounding water molecules showed that the predominant neutral fluorescein structure is quinoid, while the monoanion is carboxylic. Time-Dependent Density Functional Theory predicted the origin of electronic transitions of each species, which agreed with the spectra generated using chemometrics.

1. Introduction

C.I. Solvent Yellow 94 (Fluorescein; FSC) enjoys widespread use in many areas of science, technology and medicine [1–4]; the dye has been employed, for example, as a fluorescent probe in detecting eye diseases [5–7]. The many applications of fluorescein are related to its high absorption in the visible region, namely high fluorescence emission, low toxicity and strong interaction with biomolecules [8]. In contrast, the dye is prone to photobleaching and has a complex protonation equilibrium in the ground state. The number of acidic groups in the dye suggests that pH plays an important role in its behavior, including light absorption and emission properties, which permits fluorescein to act as a probe for specific cell environments and biological targets [9]. Fluorescein is a xanthene dye, with the central carbon bonded to the position 2- of a benzoic acid (Fig. 1).

The commercial form of fluorescein is typically either the dianion (sodium salt) or neutral form. Its protolytic equilibrium involves four species namely the dianion (F^{2-}), the monoanion (FH^-), the neutral (FH_2) form, and the cation (FH_3^+), so that three acid-base equilibria are expected. These pKa have been assigned the approximate pH values of 2, 4, and 6 [10,11].

$$FH_3^+ + H_2O \rightleftharpoons FH_2 + H_3O^+ \quad pKa_1$$
$$FH_2 + H_2O \rightleftharpoons FH^- + H_3O^+ \quad pKa_2$$
$$FH^- + H_2O \rightleftharpoons F^{2-} + H_3O^+ \quad pKa_3$$

FH_3^+ and F^{2-} are the prevalent forms at extreme pH, the first one at low pH and the dianion at high or neutral pH (Fig. 1) [10,11]. The dianion molar absorptivity in water at pH ~ 9 is high; at 490 nm, in the present work the value of 88,000 L mol^{-1} cm^{-1} was used [11–13], although a value of 76,900 L mol^{-1} cm^{-1} have been quoted [10]. This species predominates in the range applicable to human physiological media (pH ~ 7.3) [10,11]. As pH decreases, protonation leads to the monoanion FH^- (pKa_3 ~ 6), which exist as two possible tautomers, the monoanionic carboxylate (MAC) and the monoanionic phenolate (MAF) [10] (Fig. 1). Subsequent decrease in pH produces the neutral form, FH_2, that exhibits three possible structures namly a lactone (NEL), a zwitterion (NEZ) and a quinoid (NEQ). The proposition of the existence of various tautomers for

* Corresponding author. Tel.: +55 44 32613654; fax: +55 44 32614125.
E-mail address: nhioka@uem.br (N. Hioka).

0143-7208/$ – see front matter © 2009 Elsevier Ltd. All rights reserved.
doi:10.1016/j.dyepig.2009.11.002

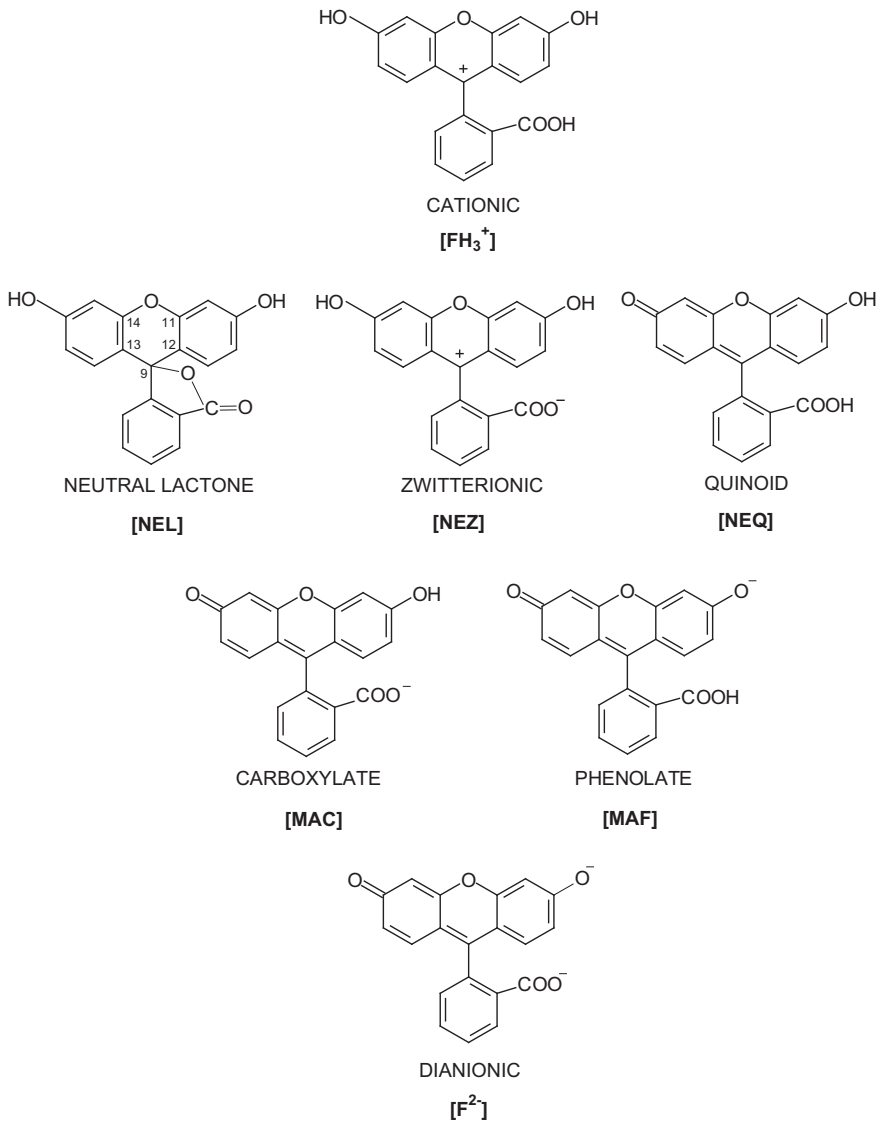

Fig. 1. FSC protolytic forms.

FH_2 is based on solid state studies, which determined that these structures show distinct diffraction patterns and IR spectra [14,15]. Additionally, the existence of the lactone (NEL) in DMSO is based on the IR detection of C=O stretching of lactones, $\nu_{max} = 1755\ cm^{-1}$ [16]. This structure was already isolated from frozen 1,4-dioxane anhydrous solutions [14]. The zwitterionic structure (NEZ) was proposed from solid Fluorescein (yellow) by IR data similarities with pyrylium salts [14,15]. However, the predominance of each tautomer in solution depends on the solvent effect.

As previously shown, the validity of pKa determination depends on the analytical method employed, including the mathematical treatment, and involves several experimental parameters, such as solvent, concentration, ionic strength, and temperature [17]. The analysis of the protolytic species of FSC by UV–Vis absorption spectrophotometry is difficult due to extensive spectral band overlapping and close pKa values. Classically, pKa estimations by UV–Vis are based on application of the univariate method in which absorption is monitored at one (or two) single wavelength(s) (the analytical wavelength(s)). However this method is recommended only in systems that presents low spectral superposition and pKa differences higher than 3 pH units ($\Delta pKa > 3$) [17]. Due to the importance of reliable pKa values for FSC, the chemometric approach could potentially be useful [10,18,19]. The chemometric approach involves analysis of all wavelengths simultaneously (full spectra), searching for the individual contributions of each species at each pH, and using many data points instead of a single analytical wavelength.

Although quantum chemical studies on protolytic FSC structures have been reported [20–27], these concern only a limited number of tautomers of each protolytic species and detailed aspects of structural parameters were unresolved. An important contribution was that of Tamulis et al. [20] who used Time-Dependent Density Functional Theory (TD-DFT) and suggested that the increased fluorescence of F^{2-} was attributable to its extensive molecular symmetry. Protonation decreases molecular symmetry and increases the number of allowed electronic states for the mono-anion (only MAC was considered), favoring the non-radiative deactivation of the excited state.

In the present work, pKa values for fluorescein were estimated using UV–Vis spectrophotometry and chemometric tools. The predominant tautomer of each protolytic species in water and vacuum were studied using several techniques based on Density Functional Theory and their electronic transition properties were characterised.

2. Experimental methods

2.1. Materials and methods

UV–Vis spectra were obtained on a Varian model Cary-50 spectrophotometer. All experiments were performed at 303.15 K. Sodium chloride 0.1 mol L^{-1} was used to control the ionic strength. The pH range investigated was between 0 and 13 using McIlvaine or boric acid or bicarbonate buffers (all 7.5 $\times$ 10^{-3} mol L^{-1}) or in HCl/NaOH standardized solutions. For buffer solutions, the final pH was measured using a Meterlab pHM 240 pH m.

The pKa were calculated considering the absorbance profile at a single wavelength (analytical wavelength) as a function of pH and the resulting data were analyzed by derivative methods (first and second order mathematical analysis) – the classic treatment [28]. Additionally a more detailed data analysis based on the chemometric approach over a full spectra (300–600 nm) was determined by the use of software [29] developed by the Chemometry Laboratory for Natural Sciences of the Universidade Estadual de Londrina, Brazil. In these cases, pKa values were determined by two equivalent methods, employing the relative protolytic concentrations calculated by chemometry: (i) pKa values corresponding to the pH where the relative concentrations of two protolytic species are equal; (ii) pKa determined by applying the relative concentrations of these two species in the Henderson–Hasselbalch equation. These two methodologies result in very similar pKa values. However, the second method was applied to obtain more accurate pKa values especially in cases in which the relative concentration curves show some experimental data dispersions.

2.2. Quantum chemical calculations

The FSC protolytic structures used in the theoretical calculation were based on the work of Sjöback et al. [10]. The structures were pre-optimized at the Hartree-Fock level, using STO-3G as the atomic basis set. Subsequently, the structures were refined by using the B3LYP hybrid functional and the 3–21+G* atomic basis set, in a vacuum and also simulating hydration by the use of the SCRF (Self–Consistent Reaction Field) Onsager Model [30]. The absence of complex vibrational frequencies confirms that these refined structures are at energy minimums. All calculations were performed on Gaussian 03 W software package [31].

Thermodynamic parameters for the isolated and solvated structures were estimated using thermochemical data furnished after calculating frequencies, based on a procedure recommended by Ochterski [32]. The excitation spectrum of each tautomer was calculated by TD-DFT [33,34] for the isolated and solvated (Onsager model) species, using the same hybrid function and the 3–21+G* atomic basis set, by calculating the first 20 singlet–singlet electronic transitions. Additionally, these structures were optimized by DFT calculations based on the B3LYP hybrid function using different atomic basis sets, and each species studied was immersed in the dielectric continuum generated by the Integral-Equation-Formalism Polarizable Continuum Method (IEFPCM) model [35,36]. After that, excitation energies were calculated using TD-DFT, the B3LYP hybrid function in combination with the IEFPCM model, and different atomic basis sets. The results were compared with those previously obtained using the Onsager model and the data estimated by chemometric analysis. The Natural Bond Orbitals (NBO) were calculated from the structures optimized in water, using the same DFT hybrid function and the 6-311G atomic basis set. The Molecular Electrostatic Potential (MEP) was generated by the software Molekel 4.3 [37,38].

3. Results and discussion

3.1. pKa determination of FSC in water

From the Fluorescein UV–Vis absorption spectra presented in Fig. 2A, it was possible to follow the protolytic processes in the pH range between 0 and 13.

The cationic species (FH_3^+) of FSC predominates in acidic water, which is evidenced by a band centered at 437 nm. In alkaline conditions (pH > 8), FSC is present as dianionic species (F^{2-}), exhibiting a band with maximum absorption at 490 nm. As shown in Fig. 2A, it is impossible to determine the spectra of the intermediate species (neutral FH_2 and monoanionic FH^-) due to extensive band superimposition. Additionally, isosbestic points are not observed in Fig. 2A, which indicates the existence of a complex protolytic equilibrium [39].

Fig. 2B exhibits the dependence between absorbance and pH monitored at some single wavelengths: 437, 452, 474, and 490 nm, these specific wavelengths are related to the regions where the cationic, neutral, monoanionic and dianionic forms of FSC absorb, respectively, as reported by Sjöback et al. [10].

The highest variation in absorbance (ΔAbs) is observed at 490 nm. Using this specific wavelength for the analysis, it was quite difficult to notice three distinct protolytic equilibria. Through the methods of first and second derivatives for the classic "S-shaped" curve, only one pKa around 6.3 was ascertained, whose value is attributed to pKa_3. At 474 nm, two pKa values were observed: $pKa_2 \sim 4.3$ and $pKa_3 \sim 6.3$. Following the absorbance at 437 and

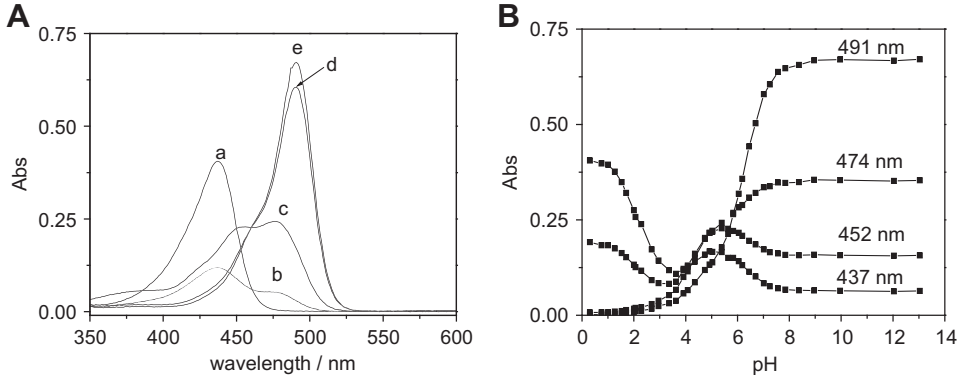

Fig. 2. A) Spectra of FSC (7.76 $\times$ 10^{-6} mol L^{-1}) in aqueous solutions at various pH values: (a) 0.31, (b) 3.36, (c) 5.39, (d) 7.25, and (e) 13.04. [NaCl] = 0.1 mol L^{-1} and 303.15 K B) Absorbance profile as a function of pH at specific wavelengths.

452 nm, three inflection points were found: (i) $pKa_1 \sim 1.9$, (ii) $pKa_2 \sim 4.4$ and (iii) $pKa_3 \sim 6.3$. All these values are in agreement with one another. However, this traditional pKa calculation, which considers only a few wavelengths, is not reliable for FSC due to the following reasons: (i) usually, the chosen wavelength is the one with the highest verifiable ΔAbs, in this case 490 nm, which unfortunately wrongly indicates only one acid-base equilibrium, (ii) extensive superimposition among the absorption bands, which affects the absorbance values of each protolytic species, (iii) the pKa difference (ΔpKa) is small, and (iv) isosbestic points could not be detected. These considerations show that the estimating pKa for the FSC protolytic system is not an easy task.

For FSC, applying the Principal Component Analysis methodology (PCA), the presence of four species explains 99.996% of the variance contained in the data, as reported in Table 1. This result suggests that the spectral set contains information on the four expected protolytic species.

By applying Q Factor analysis followed by Varimax and Imbrie Oblique Rotations [40–43], the curves of relative concentrations of the four protolytic compounds of FSC as a function of pH were determined (illustrated in Fig. 3A). The obtained values from this diagram are $pKa_1 = 2.5$, $pKa_2 = 3.8$, and $pKa_3 = 6.1$, differing from those we previously calculated using the traditional derivative method at individual wavelengths (around 1.9, 4.4 and 6.3). These methods disagree particularly for pKa_1 and pKa_2. The chemometric calculations resulted in $\Delta pKa_{(2-1)} = 1.3$ units; this close proximity of pKa_1 and pKa_2 values results in errors with the usual methodologies that are probably associated to band superimposition.

Chemometric methods based on PCA for FSC pKa determination had already been used [10,19,44,45] to obtain the curves of relative concentrations, which resulted in $pKa_1 = 2.1$, $pKa_2 = 4.3$ and $pKa_3 = 6.4$ [10,19]. These values agree somewhat with our calculations using the traditional derivative method, but differ from those determined by applying the Imbrie Q method ($pKa_1 = 2.5$, $pKa_2 = 3.8$ and $pKa_3 = 6.1$). Some of the advantages of our experimental design are the large number of samples analyzed and the low FSC concentrations employed (high concentration can induce self-aggregation in water, as occurred in porphyrin dyes [46–48]).

Additionally, these concentration curves (Fig. 3A) are relative (0–1) because they are normalized by the length unit of the most divergent spectral vectors and do not correspond to the real fractions of the species (the molar fraction of each species). To find out these molar fractions, the calculated pKa values were applied to the classical equations of mass balance for protolytic systems [49],

$$\alpha_1 = \frac{[H^+]^3}{POL}; \alpha_2 = \frac{Ka_3[H^+]^2}{POL}; \alpha_3 = \frac{Ka_3Ka_2[H^+]}{POL};$$
$$\alpha_4 = \frac{Ka_1Ka_2Ka_3}{POL}$$

and

$$POL = [H^+]^3 + [H^+]^2 Ka_3 + [H^+] Ka_3Ka_2 + Ka_3Ka_2Ka_1$$

which are the values in the diagram illustrated in Fig. 3B.

Fig. 3B shows that the cationic FH_3^+ prevails at pH < 2.5. The neutral species, FH_2, predominates in a narrow pH range (between 2.5 and 3.7) due to the proximity to pKa_1 and pKa_2. Between pH 3.8 and 6, the monoanionic FH^- prevails, while above pH 6 the dianionic F^{2-} is the main form. To illustrate the complexity of the system, the solution at pH 3 was taken as example: at this pH, FH_2 is the predominant protolytic form, however, FH_3^+ and FH^- are also present.

Applying the K-matrix method and using data from Fig. 3B, the spectra of each pure protolytic species of FSC were simulated (Fig. 4). The simulated spectra of the cationic (FH_3^+) and dianionic (F^{2-}) forms are easily compared to those experimentally determined.

As shown in Fig. 4, the FH_2 and FH^- spectra are completely superimposed by the spectra of the cation and dianion forms, similarly to the spectra reported [19]. At 490 nm (absorption maximum of F^{2-}), the FH^-, FH_2, and FH_3^+ species have low molar absorptivity, which explain the observation of only pKa_3 by using the experimental data at this wavelength. The FSC molar absorptivities (ε) at the wavelengths corresponding to the maximum absorption (λ_{max}) are shown in Table 2.

To ensure the validity of the calculated pKa values, the curve of absorbance intensity versus pH at 490 and 437 nm was constructed using the calculated molar fractions (Fig. 3B) and their molar absorption coefficients (Table 2). Theses curves were compared with the experimental data in Fig. 5.

At 490 nm, the curves show excellent agreement with experimental variation (Fig. 5). Although at 437 nm a weak correlation was obtained for the intensity, all three pKa points showed up at the same pH values. These results confirm the reliability of the chemometric methodology for pKa estimation in complex systems. Two of the most important aspects of this mathematical strategy are: (i) a calibration set (standard solutions) is unnecessary and (ii) chemical separation stages are not necessary, which decreases both experimental time and error.

Table 1
Principal component analysis for FSC spectral data.

Variables	Explained Variance (%)	Accumulated Variance (%)
1	72.3623	72.3623
2	25.3325	97.6947
3	2.2741	99.9688
4	0.0269	99.9958
5	0.0018	99.9975

3.2. Protolytic structures estimated using quantum mechanical calculation

Although FSC is a well-known compound, few studies have been devoted to basic aspects, such as the characterization of the most stable structures of each protolytic species, as already illustrated in Fig. 1. Therefore, in this work, each FSC protolytic tautomeric structure was evaluated using a method from DFT.

The Gibbs free energy of formation (ΔG_F) and other thermodynamic parameters, calculated for each optimized structure [32] in water using the Onsager model are presented in Table 3.

3.2.1. Analysis of neutral NEZ and NEL structures (FH_2)

During structure optimization either in a vacuum or in water, the NEZ structure (zwitterionic) converged to NEL (lactone), suggesting that the ΔG_F difference between both species is insignificant, though NEL is the most stable due to its electroneutrality. The relatively small difference between the charges in the zwitterionic form (NEZ) leads to formation of a cyclic structure (structures in Fig. 1), which tends to favor the stability of NEL conformation.

A detailed investigation into the optimized NEL structure shows that the distance between the oxygen and carbon (responsible for the lactone bond) is 1.55 Å, about 20% greater than the length of the C–O bond in simple lactones [50]. However, this distance agrees with the value found experimentally in solid Fluorescein [51], in

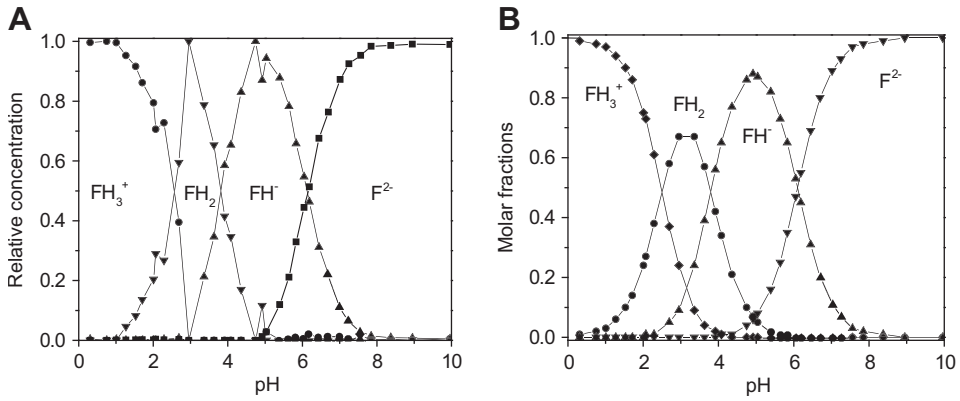

Fig. 3. Concentration curves for each FSC protolytic species versus pH: A) Relative concentrations (0–1) and B) Actual molar fraction.

some fluorescein derivatives [52], and in Rhodamines [53]. The analysis of the theoretical data suggests that the presence of the aromatic ring as a substituent increases the bond length of lactone due to steric factors.

The NBO analysis confirms the stability of the lactone bond, showing the existence of the following interactions between molecular orbitals, stabilizing the lactone bond with about 156.35 kJ mol^{-1}: $\sigma_{C13-C14} \rightarrow \sigma^*_{C9-O}$, $\sigma_{C11-C12} \rightarrow \sigma^*_{C9-O}$, $\sigma^*_{C13-C14} \rightarrow \sigma^*_{C9-O}$, $\sigma^*_{C11-C12} \rightarrow \sigma^*_{C9-O}$ (all on the pyran ring). The used carbon identification can be seen on NEL representation in Fig. 1. These results and the fact that $\Delta(\Delta G_F) \sim 0.00$ kJ mol^{-1}, suggest that NEL and NEZ should be in equilibrium or, in our proposition, that they represent the same structure.

3.2.2. Analysis of neutral NEL and NEQ structures (FH_2)

As the ΔG_F data suggests (Table 3), NEZ = NEL is the most stable structure for neutral FSC in water. The existence of NEL and NEQ in solution has a similar probability, since the $\Delta(\Delta G_F)$ between these species is very low, about 4 kcal mol^{-1}, slightly favoring NEL. The entropic parameter for both species in water has almost the same contribution. Considering that the conversion from NEL to NEQ occurs by rearrangement, the calculated Gibbs Free Energy of Reaction ($\Delta G_R = -2.97$ kJ mol^{-1}) suggests that this transformation is thermodynamically favorable. Additionally, the calculated dipole moment for both species highly favors NEQ in water (see Table 4).

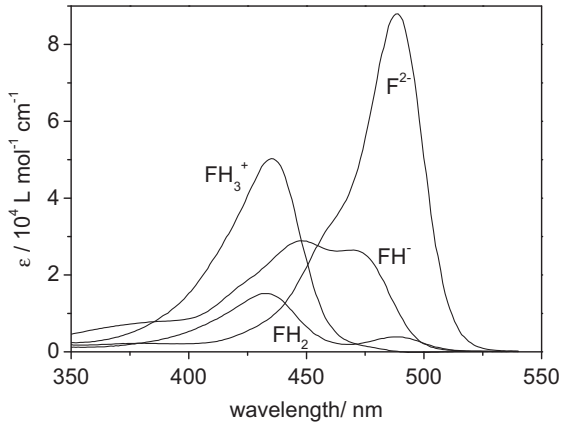

Fig. 4. Proposed spectra for the FSC protolytic species generated by the K-matrix method.

Invoking Le Chatelier's principle, NEQ is more stable in water than NEL due to the higher dipole moment of NEQ. This has a positive effect on the conversion of NEL to NEQ in water, leading to more NEQ presence in the mixture.

This seems to be a very controversial subject. Based on mathematical adjustments of electronic absorption spectra in the visible region, Klonis and Sawyer [11] reported that neutral Fluorescein in water exists as 70% lactone (NEL), 15% zwitterion (NEZ), and only 15% in the quinoid form (NEQ). Mchedlov-Petrosyan and co-workers [15,54] showed that NEL exists in DMSO and prevails in ethanol and ethanol-water mixtures. One of the first studies based on the application of quantum mechanics (DFT, based on the B3LYP hybrid functional) of FSC by Jang et al. [22] was performed in vacuum, DMSO and water. The data collected were consistent with those reported [54]. However, our NMR (^{1}H, ^{13}C, DEPT and HMQC) data for FSC suggest that NEQ is the favored structure in methanol (spectra published as Supplementary material).

3.2.3. Analysis of the monoanionic MAC and MAF structures (FH^-)

We determined that the more stable monoanion in aqueous solution is the carboxylate (MAC) from the calculated Gibbs Free Energy of Formation (see Table 3). This form is slightly more stable (0.7%) than MAF. In absolute values, $\Delta(\Delta G_F) = -18.17$ kJ mol^{-1} for MAC (Table 3). These species exhibit similar dipole moments in isolated calculations (Table 4), but MAC is slightly favored in water because its dipole moment is slightly higher. The estimated $\Delta G_R = -21.31$ kJ mol^{-1} considering unimolecular rearrangement from MAF to MAC also favors MAC, as similarly proposed in the literature [15,55]. Studies in water have shown that MAF would represent around 0.1% of the total FH^- [11]. Theoretical investigations using the B3LYP hybrid function [56] also suggest that MAC is the predominant species.

Table 2
Molar absorptivity of FSC protolytic structures at wavelengths corresponding to the λ_{max} estimated by chemometry.

Species	λ_{max} (nm)	ε (L mol^{-1} cm^{-1})
Cationic, FH_3^+	437	50,400
Neutral, FH_2	434; 488	15,100; 3900
Monoanionic, FH^-	448; 470	28,600; 26,400
Dianionic, F^{2-}	490	88,000[a]

[a] value for F^{2-} was taken as reference [11–13].

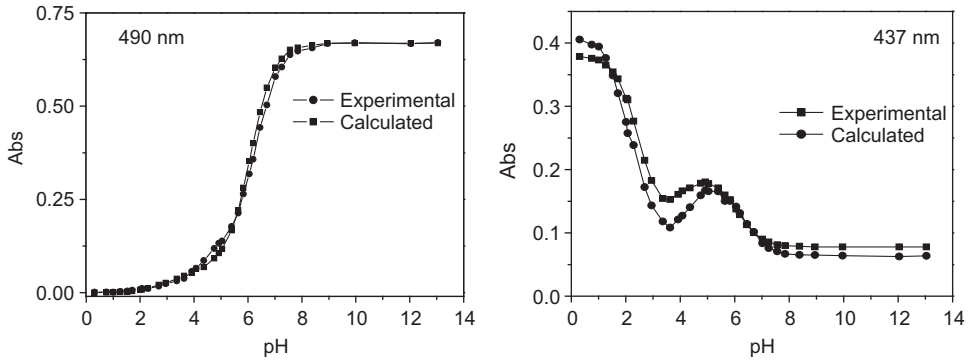

Fig. 5. Profile of the absorbance intensity versus pH for FSC: experimental and calculated values using the molar fraction and molar absorption coefficient obtained by the K-matrix method at 490 and 437 nm.

3.3. Theoretical data and pKa analysis

The quantum mechanical data for FSC tautomers have been useful in the analysis of pKa experimentally estimated in water using chemometric methods (Fig. 1). The value of 6.1 for pKa_3 corresponds to the equilibrium between MAC and F^{2-}, indicating that this protolysis is related to the phenyl group. This value is much lower than that reported for the non-substituted phenol derivatives [56] – around 10; the increased acidity of MAC is a consequence of the presence of electron-withdrawing moieties near the phenol ring (part of the xanthene ring). Electron density maps for all stable protolytic forms of FSC in water are illustrated in Fig. 6. The high electron-density portions are represented by dark red, the neutral regions by green, and electron deficient regions by dark blue. The structure of F^{2-} contains negative charges dispersed across the two oxygen atoms in the carboxylate group (Fig. 6). The pKa_3 is related to protonation that leads to the MAC form (phenolate–phenol) that causes an irregular negative density decrease over the oxygen atoms in carboxylate – asymmetric distribution over these two oxygens of the MAC form (Fig. 6). Therefore, the electron cloud on the xanthene ring affects the electron density of the carboxylate group, interfering with its protonation. This explains the lower pKa_2 of the carboxylic group for FSC (3.8) when compared to benzoic acid (around 4.2) [56]. Furthermore the xanthene ring is more electron-withdrawing than the hydrogen (benzoic acid comparison), which is responsible for the observed increment in the carboxylic acidity.

The geometric parameters of the protolytic species of FSC calculated by DFT tend to furnish a comprehensive picture of the experimental behavior [13,14,20,51,57]. Table 5 shows the values of two important dihedral angles: all stable protolytic structures have a dihedral angle between the benzene and the xanthene rings, $\phi 1$, of approximately 90°, indicating that these two rings are orthogonal. These results are in agreement with those previously mentioned in literature [58], showing that the 90° angle restricts conjugation in the xanthene so that the excited electron is confined in the xanthene with low energy dissipation, which is responsible to the high fluorescence yield [59,60]. The highest deviation from orthogonality is observed for the MAC structure, probably a consequence of the interaction between the C9 (See Fig. 1, NEL structure for atom identification) and one of the oxygen from carboxylate (Fig. 6). The $\phi 1$ angle deviates form orthogonality in 18.5° (Table 5), which result agrees with Tamulis and co-workers [20]. This weak interaction tends to lead to a cyclic structure – a lactone bond, as observed in the NEL conformation. Additionally, the angle between the benzene ring and both oxygen atoms of the carboxylate, represented as $\phi 2$, is near zero, indicating that this last group is lined up along the benzene ring, except in the case of the MAC form (4.33°), which agrees with the weak interaction previously mentioned.

3.4. Simulation of the UV–Vis absorption spectra

It is expected that the combination of an adequate atomic basis set and elaborate solvation models may accurately predict the UV–Vis absorption spectrum of a given compound using TD-DFT [33,34]. However, in the calculation of the transition energies for the dianion of FSC, employing TD-DFT, Table 6, using different atomic basis sets and two solvent models (Onsager and IEFPCM), the results show that the introduction of IEFPCM to simulate the solute hydration, in this case, did not lead to the expected improvement in the values of excitation energy. Thus, the additional computational cost needed by the combination of the IEFPCM model and more complex basis sets for these calculations is not justifiable. Although the calculated oscillator strength

Table 3
Thermodynamic parameters calculated using DFT (B3LYP/3-21 + G*) for each FSC protolytic form in water[a] at 298.15 K. The hydration was simulated using the Onsager model.

FSC protolytic form		ΔH_F° (kJ mol^{-1})	ΔS_F° (kJ mol^{-1} K^{-1})	ΔG_F° (kJ mol^{-1})
FH_3^+	CT	−3225.32	−4.86	−1871.81
FH_2	NEL	−3862.25	−4.77	−2439.81
	NEQ	−3840.15	−4.77	−2422.19
	NEZ[b]	NEZ → NEL	NEZ → NEL	NEZ → NEL
FH^-	MAF	−4065.15	−4.65	−2679.79
	MAC	−4087.96	−4.65	−2697.96
F^{2-}	DA	−4000.69	−4.52	−2646.56

[a] The data include the solvation energy.
[b] NEZ converges to NEL during the structure optimization.

Table 4
Dipole moments for some isolated and solvated FSC structures calculated using DFT (B3LYP/3–21+G*). Hydration was simulated using the Onsager model.

Form		$\mu_{isolated}$ (debye)	μ_{water} (debye)
FH_2	NEQ	11.85	20.72
	NEL	6.13	8.58
FH^-	MAC	13.00	27.60
	MAF	15.19	20.66

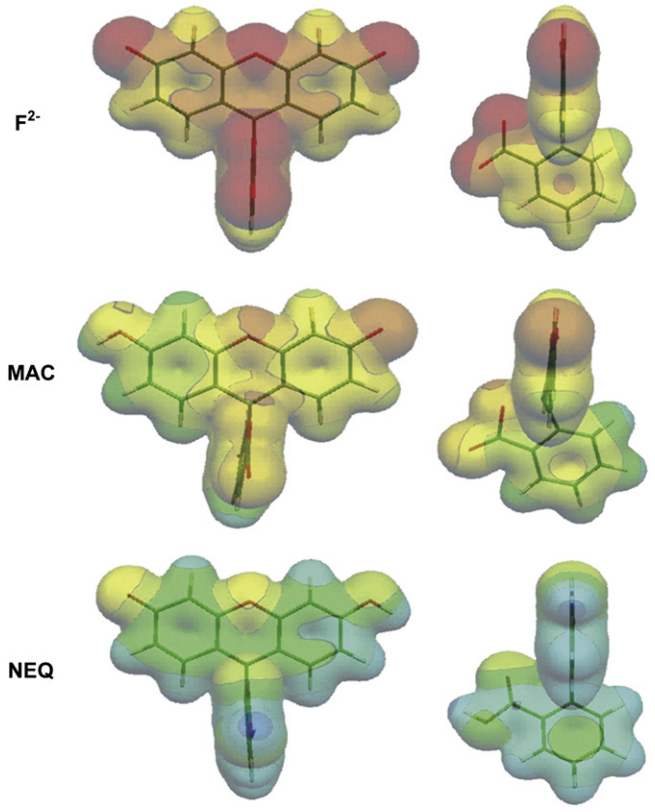

Fig. 6. Maps of Molecular Electrostatic Potential (MEP) of the most stable structure of FSC for F^{2-}, FH^{-} and FH_2 protolytic species in water (red region: higher negative charge density, green: neutrality, and blue: higher positive charge density). Frontal and lateral views. (For interpretation of the references to colour in this figure legend, the reader is referred to the web version of this article.)

converges at higher values, near 0.8, compatible with a π,π* HOMO → LUMO transition, the increased computational effort is not justified with the use of the IEFPCM model combined with more complex basis sets in this study from a quantitative point-of-view. Attempts to improve the results by associating cavities introduced by the IEFPCM model with discrete water molecules to promote specific interactions with the Fluorescein protolytic species also were not successful. This observation is likely due to the limited number of water molecules used in simulations. Novel simulations involving these surrounded by a cluster formed by water molecules and an external water cavity generated by IEFPCM model is underway.

Taking into account these aspects, the 3−21+G* basis set was used for all subsequent TD-DFT calculations. The peaks in water that we projected using this basis set can be visualized in Fig. 7.

As Fig. 7 shows, there are several calculated electronic transitions (TD-DFT) in the analyzed range for each of the structures estimated by DFT calculation, which show similarity with the spectra provided by chemometry (K-matrix method). However, as expected, the theoretical data are blue-shifted, which is probably due to underestimation of the HOMO energy by TD-DFT methods [20,61].

Table 5
Dihedral angles (φ1, between the benzene and xanthene rings and φ2, between the benzene and the carboxylate group).

Form	φ1 (°)	φ2 (°)
FH_3^+	90.39	0.49
FH_2 (NEQ)	95.72	0.70
FH^- (MAC)	108.45	4.33
F^{2-}	94.54	0.08

Table 6
Comparison between $\lambda_{exp} = 490$ nm for the dianionic FSC and the values estimated by TD-DFT using different basis sets and solvation models.

Solvation model	Basis set in the optimization	Basis set in TD-DFT calculation	λ_{max} (nm)	Deviation (%)	Oscillator strength
Onsager	3−21+G*	3−21+G*	437	−10.8	0.596
IEFPCM	6−31G(d)	6−31G(d)	428	−12.7	0.731
IEFPCM	6−31G(d)	TZVP	435	−11.2	0.770
IEFPCM	LANL2DZ	LANL2DZ	441	−10.0	0.785
IEFPCM	6−31G(d)	LANL2DZ	435	−11.2	0.770
IEFPCM	6−31G(d)	6−31G(d,p)	428	−12.7	0.731
IEFPCM	6−31G(d)	6−311++G(d,p)	437	−10.8	0.795

The most representative transitions of each protolytic species in water are presented in Table 7. The orbitals involved in each relevant transition are shown beside the wavelength differences determined by chemometry and TD-DFT methods. The oscillator strength (f), a parameter correlated to the molar absorptivity, is also presented.

The data presented in Table 7 show that the most relevant contributions to the main bands of FH_3^+, NEQ (FH_2) and F^{2-} structures involve HOMO → LUMO electronic transitions, corresponding to absorption maxima at 382, 426 and 437 nm, respectively.

3.4.1. Cationic species

As observed in Fig. 7, the absorption spectrum of FH_3^+ occurs in the visible range. It does not follow a Gaussian profile, which result is justified by the TD-DFT data (Fig. 7) that predicts the existence of two transitions, one at 382 nm (an intense HOMO → LUMO transition) and another of lower intensity at 336 nm. As can be seen, the oscillator strength (Table 7) of these bands is in agreement with the observed non-Gaussian profile.

3.4.2. Neutral species

Between the two possible structures (NEL and NEQ), it was observed that the NEL form does not contribute to the spectra in the visible region, only in the UV region (region not investigated in this study). As suggested by TD-DFT calculations, there are two relevant peaks in the spectrum of NEQ, whose ΔE (difference of energy related to these peaks positions) reasonably agrees with the one observed in the spectrum furnished by the K-matrix method. However, there is oscillator strength inversion for these peaks.

3.4.3. Monoanionic species

The correlation between the TD-DFT theoretical data and the results from K-matrix method is excellent, not showing significant signal displacement. For MAF, the multivariate K-matrix data analysis shows an intense transition at 448 nm (Fig. 4). The theoretical prediction by TD-DFT for this transition agrees very well with this value (445 nm) with a high calculated oscillator strength. MAC exhibits a low intensity band at 470 nm, whilst the TD-DFT calculation furnished one at 479 nm with a very low oscillator strength. However, the differences in intensities between the calculated oscillator strength and the K-matrix method are due to the predominance of MAC in water, as determined in the present work. Therefore, the similarity between the predominant intensities of the bands in the spectra simulated by K-matrix of the FH^- form is caused by the presence of a little MAF counterbalanced by its high molar absorptivity and much MAC compensated by its low absorptivity, as indicated by TD-DFT data.

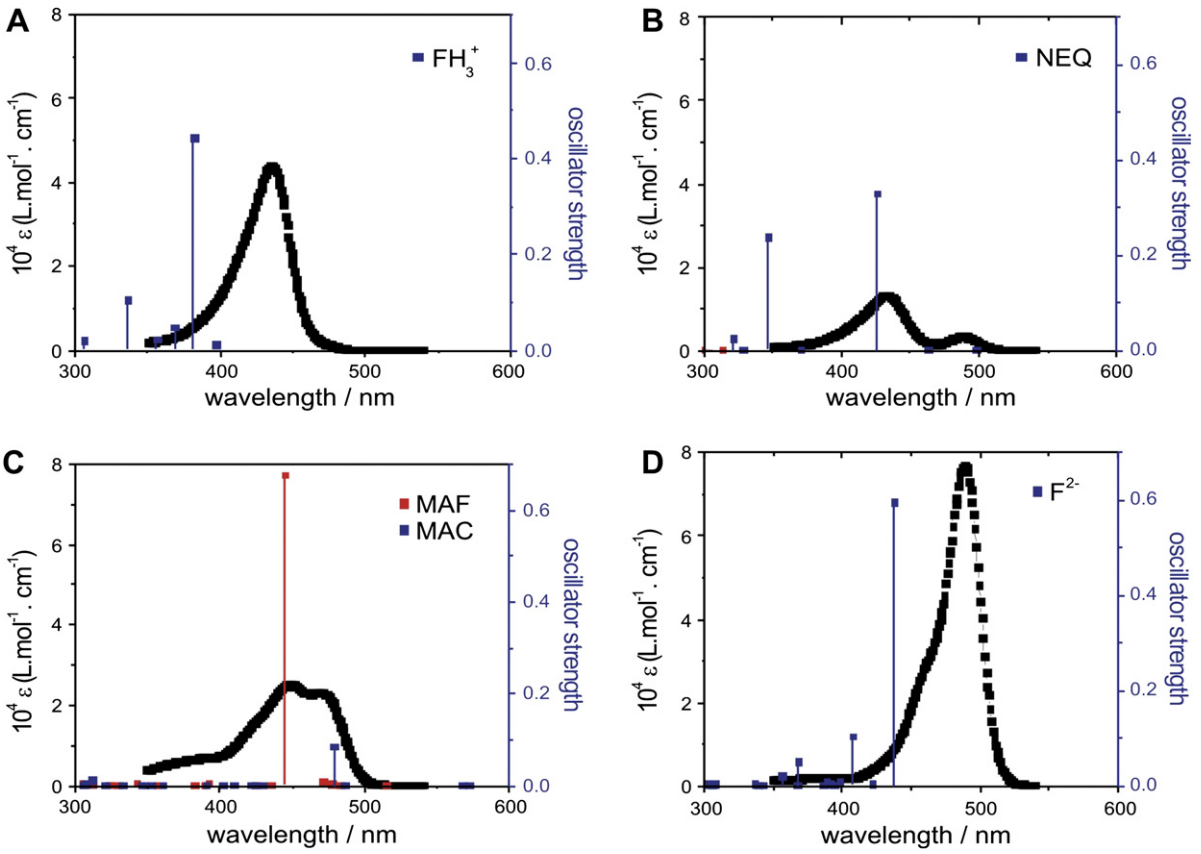

Fig. 7. Peaks calculated by TD-DFT (colored lines) and the spectra simulated by the K-matrix method (black lines) for the four protolytic forms of FSC. A) Cationic, B) Neutral (NEQ), C) Monoanionic (MAF and MAC), and D) Dianionic. (For interpretation of the references to colour in this figure legend, the reader is referred to the web version of this article.)

3.4.4. *Dianionic species*

As F^{2-} is the predominant species at physiological pH, a detailed inquiry into the origin of its spectrum becomes pertinent. The spectrum of F^{2-} shows two relevant transitions in the region between 300 and 600 nm. An intense peak with a shoulder at approximately 470 nm is experimentally observed at 490 nm. The TD-DFT data also suggest two representative signals, an intense peak at 437 nm ($f = 0.60$), followed by a low intensity peak at 407 nm ($f = 0.11$), which looks like a shoulder. The ΔE (energy difference related to these peaks positions) of the calculated and experimental results are similar. The molecular orbitals involved in the main transitions related to the absorption at 490 nm for the dianion of FSC are illustrated in Fig. 8.

The main HOMO–LUMO transition ($\Delta E_{electronic} = 292.81$ kJ mol^{-1}) for F^{2-} involves changes in the electron density of the upper carbon of the phenol ring, whose electron density shifts towards oxygen (O-10) and carbon (C-9). Once again it is showed that the electron density is restrained in the xanthene structure which justifies the high fluorescence of FSC at physiological pH [20].

The transition involving the HOMO-5 and LUMO molecular orbitals ($\Delta E_{electronic} = 406.38$ kJ mol^{-1}) also contributes to absorption at 490 nm. In this case, the electron density is directed towards the xanthene central ring (Fig. 8). However, its contribution is not relevant, as shown in Table 7 ($f = 0.11$). Again, we demonstrated that the benzene ring only minimally participates in the predominant electronic transitions for the F^{2-} species of FSC.

Table 7
Wavelengths corresponding to the λ_{max} for protolytic structures calculated by TD-DFT and the SCRF Onsager model for water, and the 3–21+G* atomic basis sets, compared to the values estimated by chemometry (*CH*).

Structure	λ_{CH}(nm)	$\lambda_{TD\text{-}DFT}$(nm)	Deviation (%) $(\frac{\lambda_{TD}}{\lambda_{CH}} - 1) \times 100$	Involved MO	Oscillator Strength (TD-DFT)
FH_3^+	437	382	−12.6	HOMO → LUMO	0.443
	416[a]	336	−19.2	HOMO-4 → LUMO	0.107
NEQ	488	426	−12.7	HOMO → LUMO	0.331
	434[a]	347	−20.0	HOMO-2 → LUMO	0.239
MAC	470	479	+1.9	HOMO → LUMO + 3	0.087
MAF	448	445	−0.7	HOMO → LUMO + 1	0.676
F^{2-}	490	437	−10.8	HOMO → LUMO	0.596
	470[a]	408	−13.2	HOMO-5 → LUMO	0.105

[a] Wavelength of the shoulder in the main absorption band.

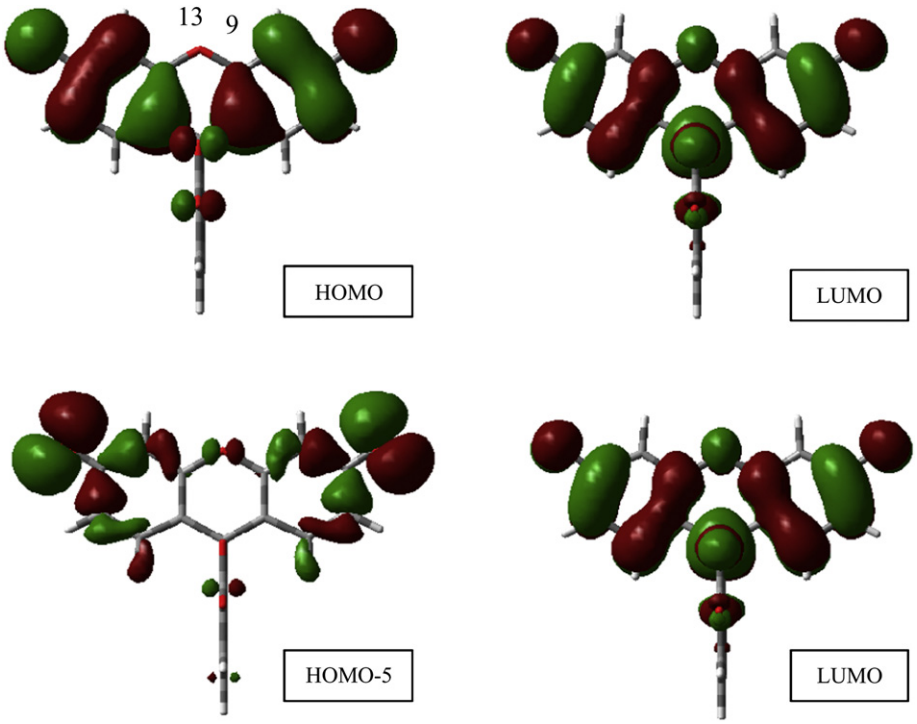

Fig. 8. Illustration of the molecular orbitals involved in the main transitions of the dianionic form of FSC related to the absorption at 490 nm.

4. Conclusions

Chemometric methods have shown to be appropriate for the study of protonation equilibria of Fluorescein in aqueous media. This system presents three pKa values, which shows high superposition of electronic absorption bands. The pKa values obtained are 2.5, 3.8 and 6.1, corresponding to pKa_1, pKa_2 and pKa_3, respectively. In addition, each protolytic species is present in solution as tautomers, whose stability depends on the solvent. Computational calculations using DFT methods allowed us to obtain the most stable protolytic structure in a vacuum and in water. In water, the predominant structure is the FH_3^+ form, the neutral one is NEQ, the monoanion is MAC, and the dianion is the F^{2-} form. The application of TD-DFT approach resulted in a reasonable explanation for the origin of the main electronic transitions of FSC, whose results are in accordance with the spectra obtained by the K-matrix method. The use of chemometric tools with model chemistry calculations maximize the quality of spectral information, leading to trustworthy FSC pKa values, which is especially useful in the analysis of complex systems.

Acknowledgements

This work was supported by grants from the following Brazilian agencies: CNPq, Fundação Araucária/Paraná State, FAPESP/São Paulo State, and FAPEMIG/Minas Gerais State. The authors are grateful to Professors Vagner Roberto de Souza and Ernani Abicht Basso (Universidade Estadual de Maringá) for their valuable suggestions, and Laerte J. da Silva for the English language revision.

Appendix. Supplementary material

Supplementary data associated with this article can be found in the online version at doi:10.1016/j.dyepig.2009.11.002.

References

[1] Tan W, Shi Z, Kopelman Y. Development of submicron chemical fiber optic sensors. Analytical Chemistry 1992;64:2985–90.
[2] Stirling RV. Video techniques in neurobiology. Trends in Neurosciences 1986;9:145–7.
[3] Walkup GK, Burdette SC, Lippard SJ, Tsien RY. A new cell-permeable probe for Zn^{2+}. Journal of the American Chemical Society 2000;122:5644–5.
[4] Setsukinai S, Urano Y, Kakinuma K, Majima HJ, Nagano T. Development of novel fluorescence probes that can reliably detect reactive oxygen species and distinguish specific species. Journal of Biological Chemistry 2003;278:3170–5.
[5] McIntyre D. The stimulation of fluorescein in external ophthalmic photography. Journal of the Biological Association 1967;35(4):155–7.
[6] Tripathi RC, Millard CB, Tripathi B. Protein composition of human aqueous humor: SDS-PAGE analysis of surgical and post-mortem samples. Experimental Eye Research 1989;48(1):117–30.
[7] Masereeuw R, Bergh E, Bindels RJ, Russel FGM. Characterization of fluorescein transport in isolated proximal tubular cells of the rat: evidence for mitochondrial accumulation. Journal of Pharmacology and Experimental Therapeutics 1994;269:1261–7.
[8] Kojima H, Nakatsubo N, Kikuchi K, Kawara S, Kirino Y, Nagoshi H, et al. Detection and imaging of nitric oxide with novel fluorescent indicators: diaminofluoresceins. Analytical Chemistry 1998;70:2446–53.
[9] Slavik J. Fluorescent probes in cellular and molecular biology. Florida: CRC Press; 1994.
[10] Sjöback R, Nygren J, Kubista M. Absorption and fluorescence properties of fluorescein. Spectrochimica Acta A: Molecular Biomolecular Spectroscopy 1995;51:L7–21.
[11] Klonis N, Sawyer WH. Spectral properties of the prototropic forms of fluorescein in aqueous solutions. Journal of Fluorescence 1996;6:147–57.
[12] Leonhardt H, Gordon L, Livingston R. Acid-base equilibria of fluorescein and 2′7′-dichlorofluorescein in their ground and fluorescent states. Journal of Physical Chemistry 1971;76(1):245–9.
[13] Mchedlov-Petrossyan NO, Bryleva EY, Vodalazkaya NA, Dissanayake AA, Ford WT. Nature of cationic poly(propylenimine) dendrimers in aqueous solutions using versatile indicator dyes. Langmuir 2008;24:5689–99.
[14] Anthoni U, Christophersen C, Nielsen PH, Püschl A, Schaumburg K. Structure of red and orange fluorescein. Structural Chemistry 1995;6(3):161–5.
[15] Markuszewski R, Diehl H. The infrared spectra and structures of three solid forms of fluorescein and related compounds. Talanta 1980;27:937–46.
[16] Mchedlov-Petrossyan NO, Mayorga RS. Extraordinary character of the solvent influence on the protolytic equilibria: inversion of fluorescein ionization constants in H_2O-DMSO mixtures. Journal of the Chemical Society, Faraday Transactions 1992;88(20):3025–32.

[17] Albert A, Serjeant EP. The determination of ionization constants. A laboratory manual. 2nd ed. London: Chapman and Hall Ltd; 1971. p. 53.
[18] (a) Lang K, Mosinger J, Wagnerová DM. Photophysical properties of porphyrinoid sensitizers non-covalently bound to host molecules; models for photodynamic therapy. Coordination Chemistry Reviews 2004;248:321–50;
(b) Sena MM, Scarminio IS, Collins KE, Collins CH. Speciation of aqueous chromium(VI) solutions with the aid of Q-mode factor analysis followed by oblique projection. Talanta 2000;53:453–61.
[19] Gholivand MB, Ghasemi JB, Saaidpour S, Mohajeri A. Spectrophotometric study of the effects of surfactants and ethanol on the acidity constants of fluorescein. Spectrochimica Acta Part A 2008;71:1158–65.
[20] Tamulis A, Tamuliene J, Balevicius ML, Rinkevicious Z, Tamulis V. Quantum mechanical studies of intensity in electronic spectra of fluorescein dianion and monoanion forms. Structural Chemistry 2003;14(6):643–8.
[21] Hirano K. Electronic structure and spectra of organic dye anions of uranine and eosin Y. Bulletin of the Chemical Society of Japan 1983;56:850–4.
[22] Jang YH, Hwang S, Chung DS. Tautomeric equilibrium of fluorescein in solution: ab initio calculations. Chemistry Letters 2001;2:1316–7.
[23] Fabian WM, Schuppler S, Wolfbeis OS. Effects of annulation on absorption and fluorescence characteristics of fluorescein derivatives: a computational study. Journal of the Chemical Society, Perkin Transactions 2 1996;29:853–6.
[24] Acemioğlu B, Arik M, Efeoğlu H, Onganer Y. Solvent effect on the ground and excited state dipole moments of fluorescein. Journal of Molecular Structure (Theochem) 2001;548:165–71.
[25] Wang L, Roitberg A, Meuse C, Gaigalas AK. Raman and FTIR spectroscopies of fluorescein in solutions. Spectrochimica Acta A: Molecular Biomolecular Spectroscopy 2001;57:1781–91.
[26] Krol M, Wrona M, Page CS, Bates PA. Macroscopic pKa calculations for fluorescein and its derivatives. Journal of Chemical Theory and Computation 2006;2(6):1520–9.
[27] Mchedlov-Petrossyan NO, Ivanov VV. Effect of the solvent on the absorption spectra and protonation of fluorescein dye anions. Russian Journal of Physical Chemistry A 2007;81(1):112–5.
[28] Previdello BAF, Carvalho FR, Tessaro AL, Souza VR, Hioka N. O pKa de indicadores ácido-base e os efeitos de sistemas coloidais. Química Nova 2006;29 (3):600–6.
[29] Março PH, Scarminio IS. Q-mode curve resolution of UV–Vis spectra for structural transformation studies of anthocyanins in acidic solutions. Analytica Chimica Acta 2007;583:138–46.
[30] Onsager L. Electric moments of molecules in liquids. Journal of the American Chemical Society 1936;58:1486–93.
[31] Frisch MJ, Trucks GW, Schlegel HB, Scuseria GE, Robb MA, Cheeseman JR, et al. Gaussian 03, revision C.02. Wallingford, CT: Gaussian, Inc; 2004.
[32] Ochterski JW. In: Thermochemistry in Gaussian, http://www.gaussian.com/g_whitepap/thermo.htm, [accessed 22.03.09].
[33] Runge E, Gross EKU. Density-functional theory for time-dependent systems. Physical Review Letters 1984;52:997–1000.
[34] Casida ME, Jamorski C, Casida KC, Salahub DR. Molecular excitation energies to high-lying bound states from time-dependent density-functional response theory: characterization and correction of the time-dependent local density approximation ionization threshold. Journal of the Chemical Physics 1998;108:4439–49.
[35] Cancès E, Mennucci B, Tomasi J. A new integral equation formalism for the polarizable continuum model: theoretical background and applications to isotropic and anisotropic dielectrics. Journal of the Chemical Physics 1997;107:3032–41.
[36] Tomasi J, Mennucci B, Cammi R. Quantum mechanical continuum solvation models. Chemical Reviews 2005;105:2999–3094.
[37] Flükiger P, Lüthi HP, Portmann S, Weber J. Molekel 4.3. Switzerland: Swiss Center for Scientic Computing; 2000–2002.
[38] Portmann S, Lüthi HP. MOLEKEL: an interactive molecular graphics tool. Chimia 2000;54:766–70.
[39] Espenson JH. Chemical kinetics and reactions mechanism. 1st ed. New York: McGraw-Hill; 1981. p. 117.
[40] Reyment RA, Jöreskog KG, Klovan JE. Geological factor analysis. Amsterdam: Elsevier; 1976.
[41] Davis JC. Statistics and data analysis in geology. 3rd ed. New York: John Wiley & Sons; 2002.
[42] Forina M, Armanino C, Lanteri S, Leardi R. Methods of varimax rotation in factor analysis with applications in clinical and food chemistry. Journal of Chemometrics 1988;3:115–25.
[43] Miesch AT. Q-mode factor analysis of compositional data. Computers and Geosciences 1976;1:147–59.
[44] Kubista M, Sjöback R, Albinson B. Determination of equilibrium constants by chemometric analysis of spectroscopic data. Analytical Chemistry 1993;65 (8):994–8.
[45] Kubista M, Sjöback R, Nygren J. Quantitative spectral analysis of multicomponent equilibria. Analytica Chimica Acta 1995;302:121–5.
[46] Chowdhary RK, Chansarkar N, Sharif I, Hioka N, Dolphin D. Formulations of benzoporphyrin derivatives in pluronics. Photochemistry Photobiology 2003;77(3):299–303.
[47] Simplicio FI, Soares RRS, Maionchi F, Santin Filho O, Hioka N. Aggregation of a benzoporphyrin derivative in water/organic solvent mixtures: a mechanistic Proposition. Journal of Physical Chemistry A 2004;108:9384–9.
[48] Tessaro AL, Fernandes DM, Terezo AJ, Souza VR, Hioka N. Influences of experimental parameters on the stability of a benzoporphyrin drug in water/ethanol mixtures: a statistical approach investigation. Journal of Porphyrins and Phthalocyanines 2005;9:609–16.
[49] Skoog DA, West DM, Holler FJ. Fundamentals of analytical chemistry. 6th ed. Fort Worth: Saunders College Pub; 1992.
[50] Briggs AJ, Glenn R, Jones PG, Kirby AJ, Ramaswamy P. Bond length and reactivity. Stereoelectronic effects on bonding in acetals and glucosides. Journal of the American Chemical Society 1984;106:6200–6.
[51] Ghelli S, Rastelli G, Barlocco D, Rinaldi M, Tondi D, Pecorari P, et al. Conformational analysis of phthalein derivatives acting as thymidylate inhibitors by means of ^{1}H NMR and quantum chemical calculations. Bioorganic and Medicinal Chemistry Letters 1996;4(10):1783–94.
[52] Neckers DC. The Indian happiness wart in the development of photodynamic action. Journal of Chemical Education 1987;64(8):649–56.
[53] Wang X, Song M, Long Y. Synthesis, characterization, and crystal structure of the lactone form of rhodamine B. Journal of Solid State Chemistry 2001;156:325–30.
[54] Samoilov DV, Mchedlov-Petrosyan NO, Martynova VP, El'tsov AV. Protolytic equilibria of fluorescein nitro derivatives. Russian Journal of General Chemistry 2000;70(8):1343–57.
[55] Mchedlov-Petrossyan NO, Kleshchevnikova VN. Influence of the cetyltrimethylammonium chloride micellar pseudophase on the protolytic equilibria of oxyxanthene dyes at high bulk phase ionic strength. Journal of the Chemical Society, Faraday Transactions 1994;90(4):629–40.
[56] Lide DR. CRC handbook of physics and chemistry. 85th ed. New York: CRC Press; 2005.
[57] Wang L, Roitberg A, Meuse C, Gaigalas AK. Raman and FTIR spectroscopies of fluorescein in solutions. Spectrochimica Acta A: Molecular and Biomolecular Spectroscopy 2001;57:1781–91.
[58] Osborn S, Rogens D. The crystal and molecular structure of the 1:1 complex of acetone with the lactoid form of fluorescein. Acta Crystallographica B 1975;31:359–64.
[59] Miura T, Urano Y, Tanaka K, Nagano T, Ohkubo K, Fukuzumi S. Rational design principle for modulating fluorescence properties of fluorescein-based probes by photoinduced electron transfer. Journal of the American Chemical Society 2003;125:8666–71.
[60] Ueno T, Urano Y, Setsukinai K, Takakusa H, Kojima H, Kikuchi K, et al. Rational principles for modulating fluorescence properties of fluorescein. Journal of the American Chemical Society 2004;126:14079–85.
[61] Belletête M, Wakim S, Leclerc M, Durocher G. Emission energies and photophysical properties of ladder oligo(*p*-aniline)s. Journal of Molecular Structure (Theochem) 2006;760:147–52.